Atmospheric Environment 206 (2019) 170–182

Contents lists available at ScienceDirect

Atmospheric Environment

journal homepage: www.elsevier.com/locate/atmosenv

Exploring the influence of two inventories on simulated air pollutants during winter over the Yangtze River Delta

Tong Sha[a], Xiaoyan Ma[a,*], Hailing Jia[a], Ronald J. van der A[b,c], Jieying Ding[b,c], Yanling Zhang[d,e], Yunhua Chang[d,e]

[a] Key Laboratory of Meteorological Disaster, Ministry of Education (KLME)/Joint International Research Laboratory of Climate and Environment Change (ILCEC)/ Collaborative Innovation Center on Forecast and Evaluation of Meteorological Disasters (CIC-FEMD)/Key Laboratory for Aerosol-Cloud-Precipitation of China Meteorological Administration, Nanjing University of Information Science & Technology, Nanjing, 210044, China

[b] Research & Development Satellite Observations, Royal Netherlands Meteorological Institute, De Bilt, the Netherlands

[c] KNMI-NUIST Center for Atmospheric Composition, School of Atmospheric Physics, Nanjing University of Information Science & Technology, Nanjing, China

[d] Yale–NUIST Center on Atmospheric Environment, International Joint Laboratory on Climate and Environment Change (ILCEC), Nanjing University of Information Science & Technology, Nanjing, 210044, China

[e] Jiangsu Provincial Key Laboratory of Agricultural Meteorology, College of Applied Meteorology, Nanjing University of Information Science & Technology, Nanjing, 210044, China

ARTICLE INFO

Keywords:
Emission inventory
Air pollutants
$PM_{2.5}$
WRF-Chem
YRD

ABSTRACT

Currently, haze events in winter occur more frequently than decades ago, especially in Eastern and Central China, including the Yangtze River Delta (YRD). WRF-Chem is applied in this study to explore the discrepancies of the simulated air pollutants induced by employing different emission inventories, particularly during haze events. Two inventories are involved in this study, MEIC (Multi-resolution Emission Inventory for China) and GlobEmission (inventory from GlobEmission project emission estimates), representing the emission inventories based on quite different ways. We first compared monthly emissions of SO_2 and NO_x in two inventories during January over YRD, and found the mean differences of SO_2 (NO_x) are 20% (7%), with the ranges of 0%–47% (−100%–100%). The largest differences are both found in Shanghai, with 47% for SO_2 (MEIC in 2010, GlobEmission in 2014), and 45% for NO_x (MEIC in 2010, GlobEmission in 2015), respectively, partly because the reduction of emissions was large during the 12th Five-Year Plan (2011–2015) in this area. By comparing the simulated air pollutants mass concentrations using two inventories with in-situ observations during January 2015, we found that the simulated SO_2 using MEIC and GlobEmission are both higher than observations, with mean normalized biases of 207% and 121% over YRD, respectively, and much larger in the city cluster of Nanjing-Shanghai, where are nearly four (MEIC) and three times (GlobEmission) higher than observations. In contrast, NO_2 simulations using GlobEmission are lower than observations (22%) and MEIC simulations (45%) over YRD. The largest biases of GlobEmission simulation are found in Zhejiang province (over 70%). The biases of simulated monthly mean $PM_{2.5}$ are 38% (MEIC) and 30% (GlobEmission) over YRD, respectively. A case study during heavy haze event shows that the biases increase to 61% (MEIC) and 39% (GlobEmission), and spatial correlation coefficient in the simulation using GlobEmission increase to 0.69 over YRD. Temporal correlation coefficients in the city cluster of Nanjing-Shanghai increase from 0.5 (MEIC) to 0.7 (GlobEmission).

1. Introduction

More frequent occurrence of haze events with extremely high $PM_{2.5}$ concentrations in China during wintertime has drawn a lot of attention in recent years. Yangtze River Delta (YRD) region is one of the most densely populated and fastest economically growing areas in China and has been suffering from severe air pollution. For instance, four haze episodes occurred and affected many cities in the YRD during January 2015, which caused serious health damage and economic loss. Many field observations and modeling studies have investigated the formation mechanism of heavy haze (Wang et al., 2015a; Zhang et al., 2015; Fu et al., 2016a, 2016b; Sun et al., 2016; Zheng et al., 2016), such as high emissions of primary air pollutants, stagnant weather conditions, regional pollution transport and fast gas-to-particle conversion, while the

* Corresponding author.
E-mail address: xma@nuist.edu.cn (X. Ma).

https://doi.org/10.1016/j.atmosenv.2019.03.006
Received 9 October 2018; Received in revised form 5 March 2019; Accepted 7 March 2019
Available online 13 March 2019
1352-2310/

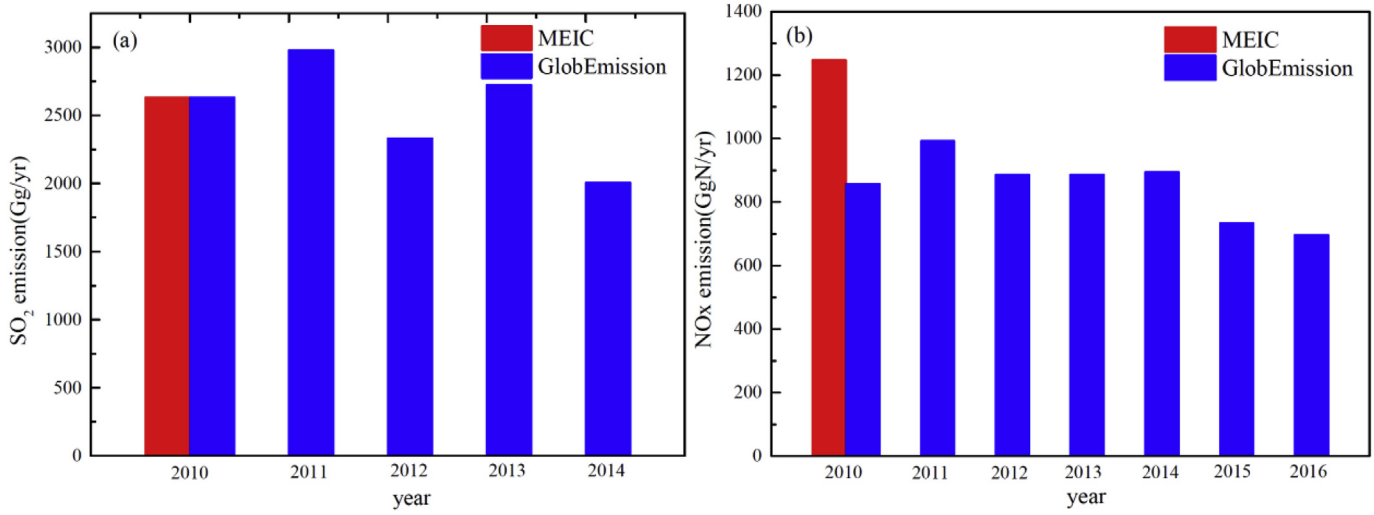

Fig. 1. Total annual SO_2 and NO_x emissions in YRD from MEIC and GlobEmission inventories (unit: Gg yr^{-1} for SO_2, Gg N yr^{-1} for NO_x).

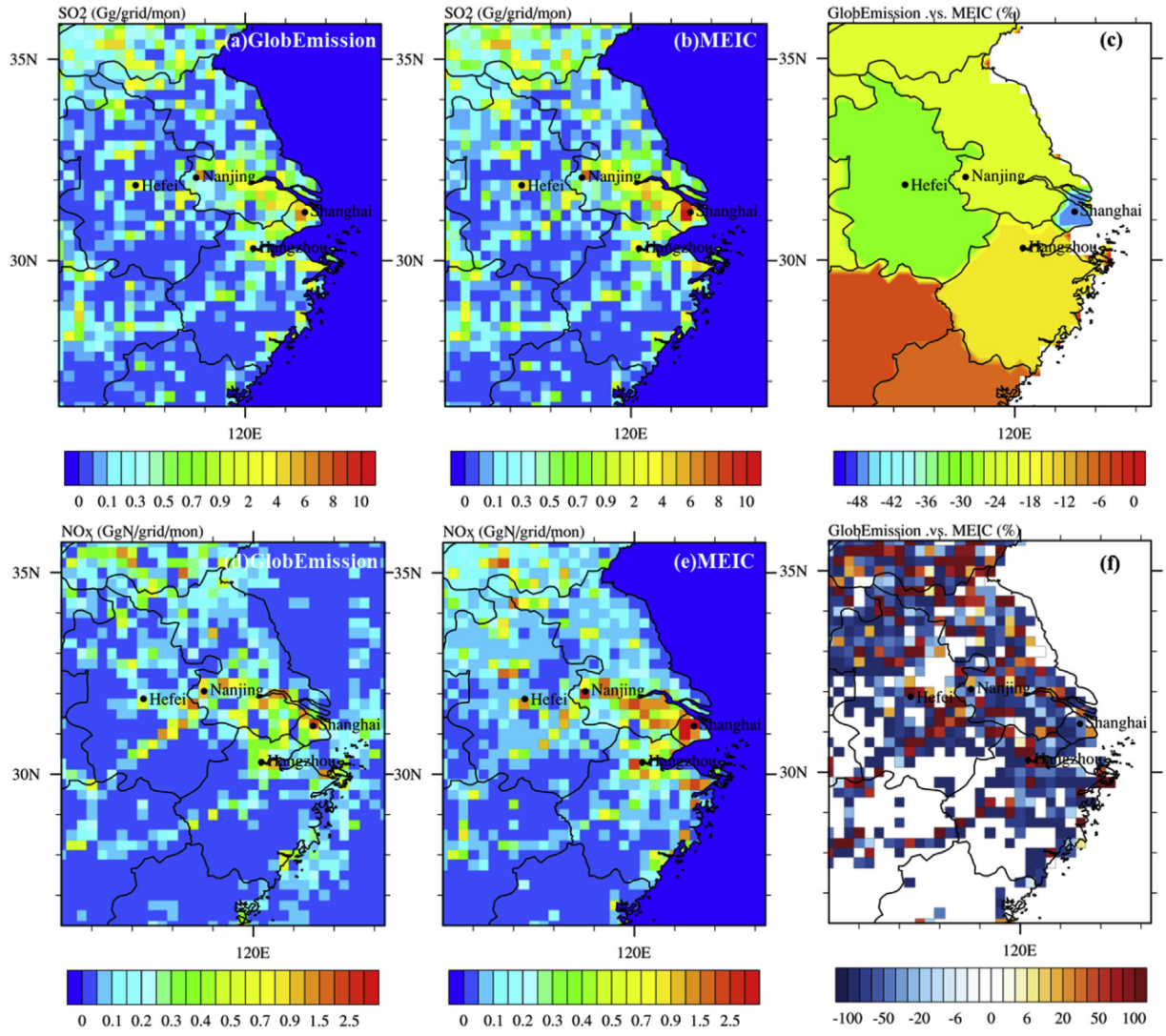

Fig. 2. Spatial distributions of monthly emissions for SO_2 and NO_x from GlobEmission inventory (a, d) and MEIC inventory (b, e) (unit: Gg $grid^{-1}$ mon^{-1} for SO_2, Gg N $grid^{-1}$ mon^{-1} for NO_x), and the differences between GlobEmission and MEIC (c, f) during January.

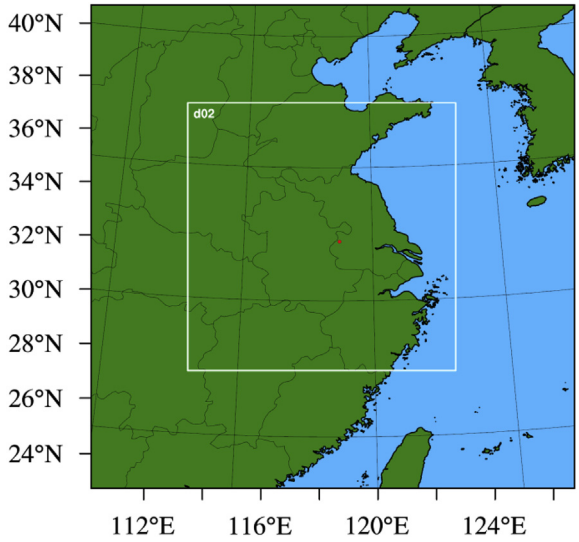

Fig. 3. The model domains (The red solid circle represents the location of Nanjing). (For interpretation of the references to colour in this figure legend, the reader is referred to the Web version of this article.)

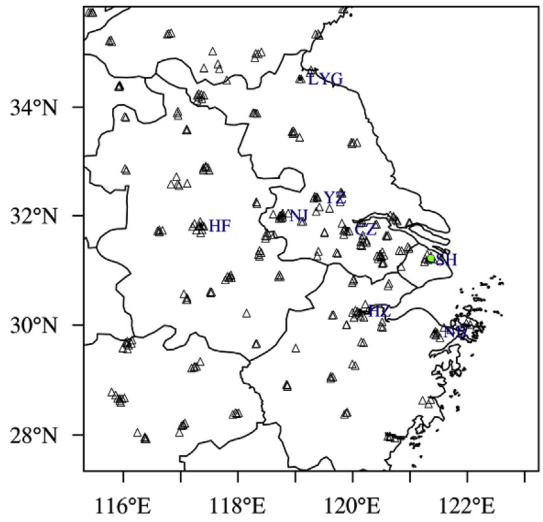

Fig. 4. Location of sites with in-situ measurements on air pollutants (Triangles denote 282 air quality monitoring sites of the MEP network, a green solid circle denotes Pudong site in Shanghai which measures hourly aerosol inorganic chemical components). (For interpretation of the references to colour in this figure legend, the reader is referred to the Web version of this article.)

causes are still not well understood. Some previous studies show that the rapid increase of secondary aerosols is considered to be one of the main causes of haze events in China. Wang et al. (2014a,b) found that sulfate, nitrate, and ammonium increased rapidly and contributed almost half of the total $PM_{2.5}$ concentrations during the haze episode in 2013 over North China Plain. Chen et al. (2016) and Gao et al. (2016a, 2016b) illustrated that secondary pollutants became the major components of $PM_{2.5}$ and increased significantly from non-haze to haze days. Numerical models are favorable tool to predict air pollutants and understand physical and chemical processes. However, large uncertainties still remain in model predictions of air pollutants, which may be caused by unclear and/or inaccurate physical and chemical mechanisms associated with air pollutants, e.g. heterogeneous chemistry (Cheng et al., 2016; Wang et al., 2016; Guo et al., 2017; Li et al., 2017a), uncertainties in meteorological conditions, as well as uncertainties of emission inventory.

Currently, the Multi-resolution Emission Inventory for China (MEIC) emission inventory developed by Tsinghua University is often used in the numerical model for air quality studies over China (Chang et al., 2016; Gao et al., 2016b; Sun et al., 2016; Li et al., 2017a; Zhou et al., 2017). The emissions of air pollutants are publicly provided for three years (2008, 2010 and 2012), which have probably changed since then due to control policy. Studies indicate that SO_2 emissions have decreased by at least 30% in recent years, especially after 2010–2011, from both bottom-up emission inventories (Lu et al., 2011; Chen et al., 2016; Xia et al., 2016) and satellite observations (Wang et al., 2015b; Krotkov et al., 2016, van der A et al., 2017), due to effective emission control and the increase of fuel combustion efficiency by promoting desulfurization technology and optimization of power plants operation. The emissions of NO_x based on various methods including bottom-up, top-down, and satellite observations all indicate an increasing tendency nationwide before 2011 (Zhang et al., 2012; Mijling et al., 2013; Xia et al., 2016). Satellite observations show that NO_x emissions reach a peak in 2011 over eastern China and then start to decrease in 2012 (Krotkov et al., 2016), which is consistent with the control policy that the Chinese government firstly set a target for 10% reduction of NO_x emission during the 12th Five-Year Plan (2011–2015). Therefore, the discrepancy between the baseline year of inventories and the years afterwards may lead to deviations of the simulated results. The estimations based on satellite observations have advantages over bottom-up emission inventories, since the former are spatially consistent and in high temporal resolution, and thus can be updated shortly after the satellite data become available.

In order to reduce the uncertainties from emission inventories, it is necessary to understand the impact of different emission inventories on the simulated air pollutants. Two inventories, MEIC and GlobEmission, representing the emission inventories based on quite different ways, are used in this study. MEIC is based on typical bottom-up approach while GlobEmission is representative of top-down inventory, in which the emissions are estimated from satellite retrievals. The main purpose of this study is to explore the differences in the simulated $PM_{2.5}$ from two inventories during winter over YRD, especially during haze event. The emissions of SO_2 and NO_x in GlobEmission have been discussed in previous studies (Ding et al., 2017a, b), the discrepancies of the emissions in comparisons to other inventories (e.g. MEIC) and its impact on the simulated $PM_{2.5}$, particularly during winter haze event over heavy polluted regions such as YRD, still remains unclear.

The paper is organized as below. We will briefly introduce the two inventories (MIEC and GlobEmission) and compare SO_2 and NO_x emissions over YRD in section 2. The description and configuration of model, as well as the introduction of in-situ measurements and meteorology evaluation, are presented in section 3. The simulations based on MEIC and GlobEmission by WRF-Chem, the impact of the two inventories on simulated air pollutants during January 2015, and a selected heavy haze event are analyzed in section 4. The summary and discussion are given in section 5.

2. Emission inventories

2.1. MEIC

Multi-resolution Emission Inventory for China (MEIC: http://www.meicmodel.org/) is a bottom-up inventory framework developed by Tsinghua University, in which a technology-based methodology was used to calculate activity data, such as fuel consumption or industrial production, emission factors of combustion or production technology, and penetration rate and emission reduction efficiency of emission controls (Zhao et al., 2014; Saikawa et al., 2017). Activity rates are derived from local provincial statistics in China and emission factors are derived from the best available local measurements and recent peer-reviewed data for China. The monthly gridded emissions are generated by applying source-based spatial and temporal profiles (Li et al., 2018). Provincial emissions are firstly distributed to counties, then further

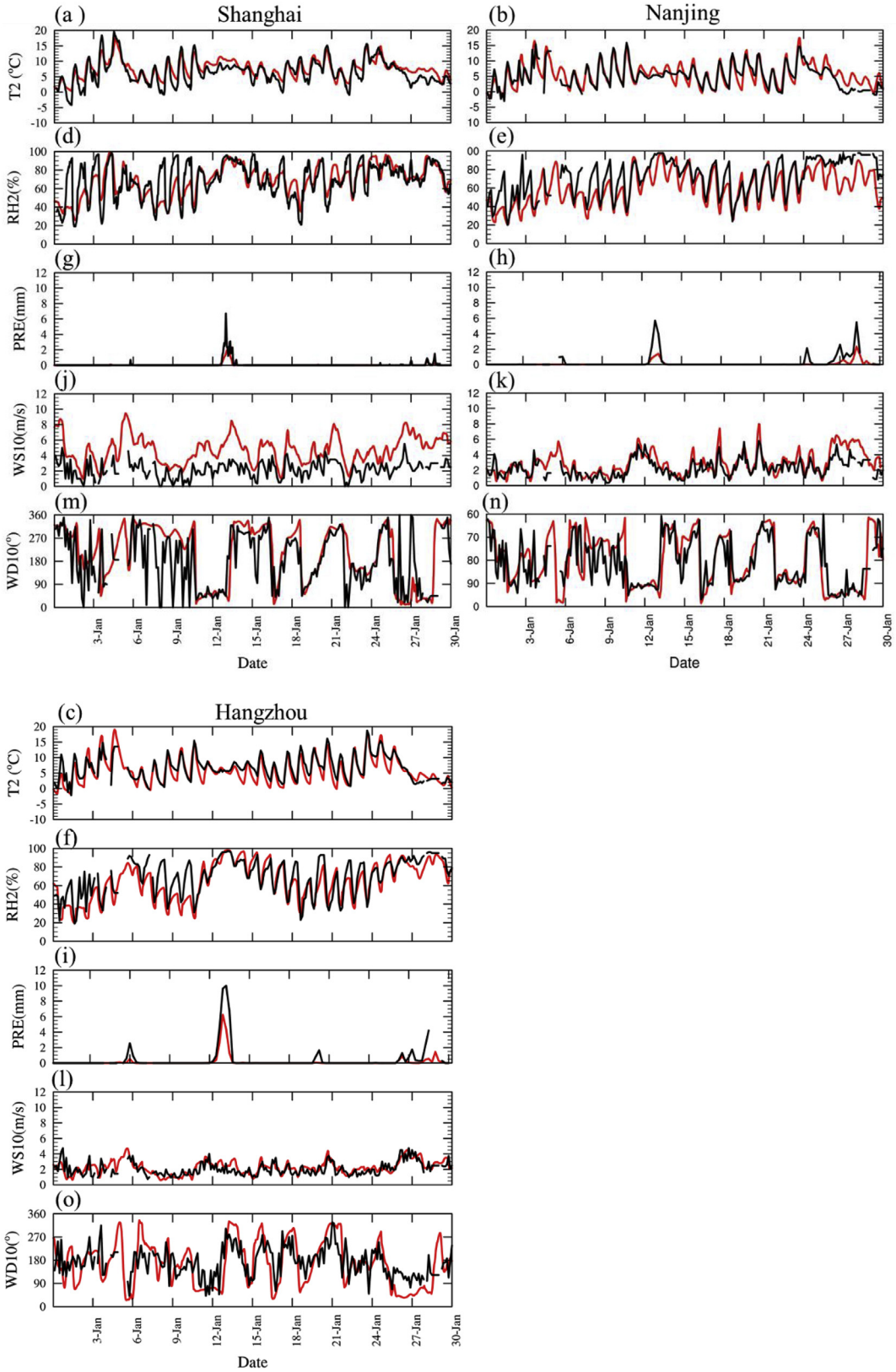

Fig. 5. Simulated (red line) and observed (black line) hourly temperature (T2) (ãc), relative humidity (RH2) (d ~ f), precipitation (PRE) (g ~ i), wind speed (WS10) (j ~ l) and wind direction (WD10) (m ~ o) at Shanghai, Nanjing, and Hangzhou. (For interpretation of the references to colour in this figure legend, the reader is referred to the Web version of this article.)

distributed to grids. The former process is based on statistics of county (i.e., GDP (gross domestic product), industrial GDP, total population, urban population, rural population, agricultural activity, vehicle population), and the latter is based on gridded maps as spatial proxies (i.e., population density map, road network). The emissions source sectors provide ten major air pollutants (SO_2, NO_x, CO, NMVOC, NH_3,

Table 1
Statistical metrics for meteorological variables during January 2015 at three cities (Shanghai, Nanjing, and Hangzhou) over YRD. (σ: standard deviations, T2: 2 m temperature (°C), RH2: 2 m relative humidity (%), WS10: 10 m wind speed ($m\ s^{-1}$)).

Variables		Shanghai	Nanjing	Hangzhou
T2	Obs(σ)	6.5(4.0)	5.2(3.9)	6.7(3.9)
	Mod(σ)	7.5(3.0)	5.6(3.6)	5.9(4.1)
	MB	1.0	0.4	−0.8
	RMSE	2.18	2.22	2.21
RH2	Obs(σ)	69.2(19.1)	71.9(19.3)	69.7(19.2)
	Mod(σ)	68.5(16.6)	60.9(17.8)	64.4(19.6)
	MB	−0.7	−11.0	−5.3
	RMSE	13.5	16.5	13.3
WS10	Obs(σ)	2.2(1.1)	2.3(1.1)	2.1(0.9)
	Mod(σ)	4.7(1.8)	2.8(1.5)	2.3(0.8)
	MB	2.5	0.5	0.2
	RMSE	2.8	1.7	0.8

CO_2, $PM_{2.5}$, PM_{10}, BC, OC) from five sources such as power, industry, residential, transportation and agriculture. Li et al. (2017b) found that typical uncertainties of 12%–31% for SO_2, 31%–37% for NO_x and 107%–133% for $PM_{2.5}$ in bottom-up inventories over China. Uncertainties mainly come from activity statistics and control measures, such as the FGD (flue-gas desulfurization) device penetration rate and removal efficiency, LNB (low-NO_x burner) application rate and abatement efficiency in power plants, emission factors of industrial boilers and various vehicle types, and vehicle fleet (Li et al., 2018). In addition, the emission factors and activities are changing quickly with time due to the rapid implementation of new technologies and air quality control regulations for power plants and vehicles in China, which make bottom-up emission inventories outdated and more uncertain (Zheng et al., 2014; Liu et al., 2015).

Users can get access to the monthly gridded emissions of three spatial resolutions (0.25°, 0.5°, 1°) for the year 2008, 2010 and 2012. Since the differences of emissions in 2010 and 2012 from MEIC inventories are quite small, the monthly emissions at 0.25° × 0.25° generated from MEIC v1.2 in 2010 are used in this study.

2.2. GlobEmission

GlobEmission project, part of Data User Element program of ESA (http://www.globemission.eu/index.php), aims to develop emissions estimated from satellite observations of air constituents and has been used in the MarcoPolo inventory by applying the sector-split of MEIC (power, industry, residential, transportation) (http://www.marcopolo-panda.eu/). The derived SO_2 emissions over China use space-based observations of SO_2 vertical columns densities from the Ozone Monitoring Instrument on board the Aura satellite, OMI/Aura, which are retrieved by using the Royal Belgian Institute for Space Aeronomy (BIRA) algorithm (Theys et al., 2015). The driving SO_2 emissions have been provided by MEIC in 2010, and then adjusted by applying a ratio, based on the variation tendency of satellite observations, to MEIC inventory on a provincial level (Koukouli et al., 2017). Therefore, the uncertainties of SO_2 emissions derived by the above methods mainly come from the driving SO_2 emissions inventory and the observed SO_2 vertical column densities from satellite.

The NO_x emissions are estimated by the Daily Emission estimates Constrained by Satellite Observation (DECSO version 5) algorithm based on extended Kalman filter. DECSO uses the CHIMERE model on a 0.25° resolution to calculate the local and non-local sensitivities of column concentration to gridded emission, together with OMI tropospheric NO_2 column data based on the DOMINO version 2 retrieval algorithm as a constraint to update emissions (Boersma et al., 2011). A more detailed description of DECSO algorithm can be found in Mijling and van der A (2012), Mijling et al. (2013) and Ding et al. (2015, 2017b). Note that the accuracy of emissions largely depends on the accuracy of the satellite-retrieved NO_2 and the chemical transport model (CTM) used in the inversion. The biases in NO_2 tropospheric columns of DOMINO version 2 are partly due to the shielding effect of high aerosol loading (Shaiganfar et al., 2011; Chimot et al., 2016), the calculation of air mass factor for retrievals at large solar zenith angles by the radiance transfer model (Lorente et al., 2017), and the estimated stratospheric background. In addition, the biases from the descriptions of chemistry, transport, and removal processes in the CTM cannot be ruled out.

In this study, emissions of SO_2 at 0.25° × 0.25° spatial resolution during January 2014 in China (the latest SO_2 emission inventories are available for 2014) and emissions of NO_x at same spatial resolution during January 2015 over East China are used for simulation. The emissions of other species come from MEIC 2010 inventory.

2.3. Comparisons of two emission inventories

Emissions inventories of air pollutants are crucial information for policy maker and are also important for simulations of air pollutants. However, large uncertainties exist in emissions estimates, so it is essential to assess different inventories for a better understanding of air pollution over China.

2.3.1. Annual mean

Fig. 1 shows annual mean emissions of SO_2 and NO_x over YRD. SO_2 emissions in 2010 are identical in MEIC and GlobEmission because the driving SO_2 emissions in the latter are based on the former inventory, while NO_x emissions in GlobEmission are 31% lower than MEIC. Lower NO_x emissions in GlobEmission have also been reported by Ding et al. (2017a). It should be noted that NO_x emissions in GlobEmission are total emissions from both anthropogenic, biogenic, and shipping emissions, while MEIC only from anthropogenic emissions. The inter-annual variations in GlobEmission show that the maxima SO_2 emissions occur in 2011, up to 2979 $Gg\ yr^{-1}$, while the minimum in 2014, only 2005 $Gg\ yr^{-1}$. Similarly, the highest NO_x emissions are also found in 2011, up to 993 $Gg\ yr^{-1}$. The NO_x emissions between 2012 and 2014 are quite close to that in 2010, followed by the lowest in 2015 and 2016, which is mainly due to the control of NO_x emissions in the 12th Five-Year Plan (2011–2015) (Zhang et al., 2018).

2.3.2. Spatial distribution

Fig. 2 shows the spatial distributions of monthly emissions for SO_2, NO_x and their differences between MEIC and GlobEmission (i.e. (GlobEmission-MEIC)/MEIC × 100%). It is shown that the spatial distributions of SO_2 emissions from two inventories are quite consistent, with high emissions in the southern Jiangsu to northern Zhejiang and Shanghai, where are the most industrially advanced and densely populated region over YRD. In addition, the differences of spatial distributions between two inventories are dependent on regional division, since SO_2 emissions in GlobEmission are estimated by multiplying a ratio to MEIC inventory on a provincial level, which is based on the variation tendency of SO_2 column concentrations from satellite observations. The differences range from 0% to 47% during January over YRD, with the mean value of 20%. The largest differences are found in Shanghai, up to 47%, followed by Anhui province (29%), while the smallest differences in Jiangsu and Zhejiang province, with only 20% and 16%, respectively.

Similar to SO_2, NO_x high emissions are also concentrated in the southern Jiangsu to northern Zhejiang and Shanghai (shown in Fig. 2d and e). Different algorithms are used for SO_2 and NO_x in GlobEmission. An advanced inversion technique, DECSO, which based on the Kalman filter, was used to estimate NO_x emissions. This inversion method can detect new emission sources which are not included in the MEIC

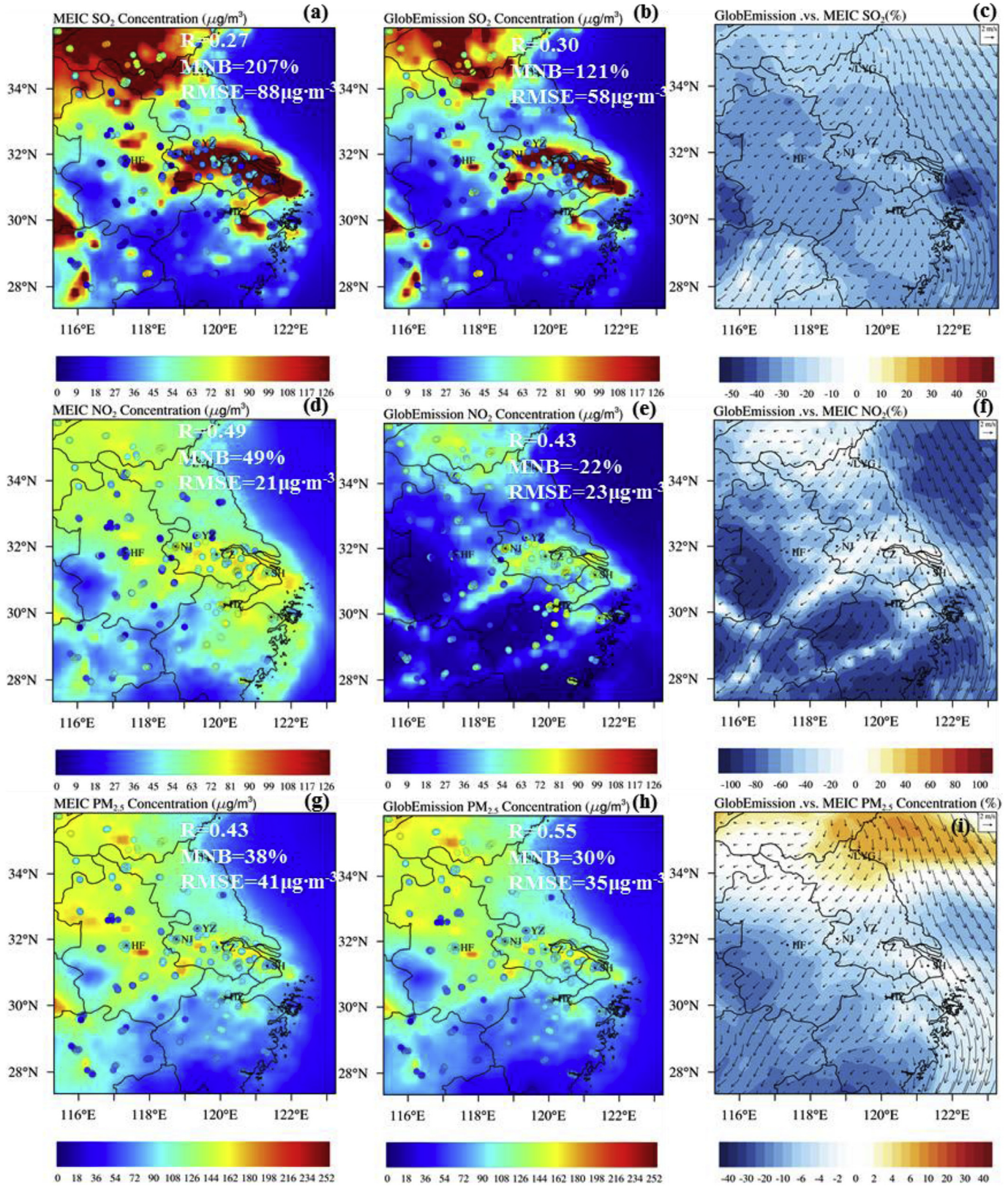

Fig. 6. Spatial distribution of simulated and observed monthly mean SO_2 (a, b), NO_2 (d, e), $PM_{2.5}$ (g, h) concentrations (unit: μg m^{-3}), and the relative differences of simulated SO_2 (c), NO_2 (f), $PM_{2.5}$ (i) using GlobEmission and MEIC ((GlobEmission-MEIC)/MEIC × 100%) during January over YRD (unit: %). (The circles represent the observed air pollutants concentrations, and the black arrows indicate simulated surface wind fields.)

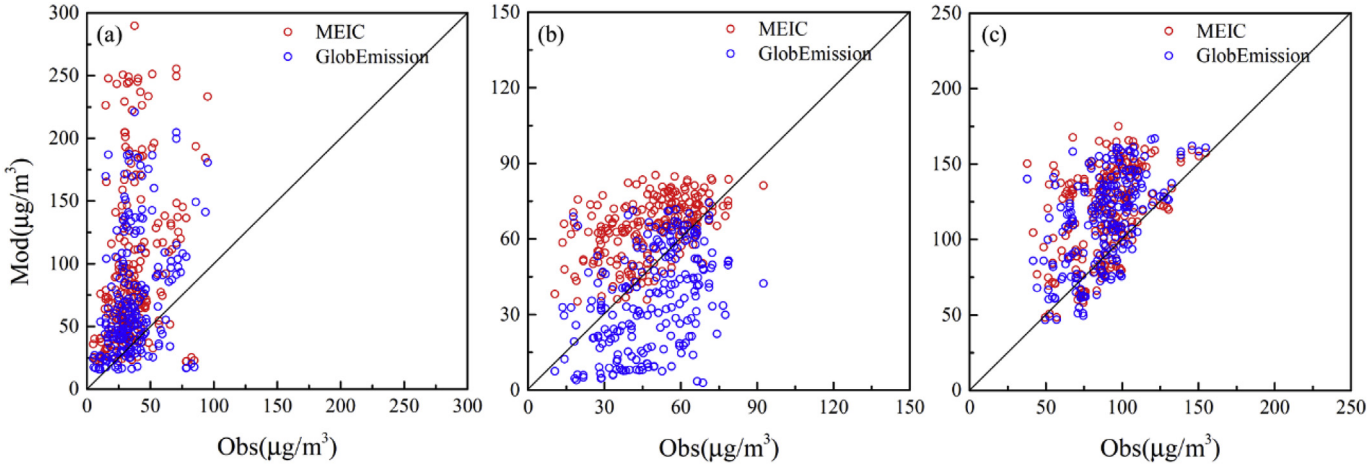

Fig. 7. Scatter plots of monthly mean SO_2 (a), NO_2 (b), and $PM_{2.5}$ (c) concentrations between simulations and observations during January over YRD (unit: μg m^{-3}). The black solid line in the graph is 1:1 line.

Table 2
The monthly mean concentrations (Avg, μg m^{-3}) and standard deviations (σ, μg m^{-3}) (in brackets) of SO_2 from observations and simulations using MEIC and GlobEmission (GE) inventories in 8 cities of YRD during January (NJ: Nanjing, LY: Lianyungang, YZ: Yangzhou, CZ: Changzhou, SH: Shanghai, HZ: Hangzhou, NB: Ningbo, HF: Hefei). Correlation coefficients (R) and mean normalized bias (MNB, %) between observations and simulations are also shown in the table.

	OBS	MEIC			GE		
	Avg(σ)	Avg(σ)	R	MNB	Avg(σ)	R	MNB
NJ	31(19)	118(142)	0.44	281	86(107)	0.43	177
LY	43(26)	42(48)	0.63	−2	33(36)	0.63	−23
YZ	34(24)	82(125)	0.39	141	61(94)	0.37	79
CZ	41(25)	212(207)	0.45	417	158(153)	0.44	285
SH	35(21)	159(157)	0.47	354	92(94)	0.53	163
HZ	25(13)	55(41)	0.37	120	40(29)	0.38	60
NB	27(17)	51(45)	0.24	89	36(33)	0.26	33
HF	28(11)	75(62)	0.42	168	53(44)	0.41	89

Table 3
Same as Table 1, but for NO_2.

	OBS	MEIC			GE		
	Avg(σ)	Avg(σ)	R	MNB	Avg(σ)	R	MNB
NJ	67(30)	70(38)	0.73	4	48(37)	0.67	−28
LY	42(20)	47(39)	0.78	12	25(25)	0.59	−40
YZ	37(23)	60(40)	0.72	62	38(45)	0.58	3
CZ	53(28)	77(36)	0.78	45	60(45)	0.73	13
SH	63(32)	70(35)	0.74	11	52(41)	0.77	−17
HZ	63(22)	59(27)	0.23	−6	19(16)	0.26	−70
NB	62(27)	61(34)	0.56	−2	16(16)	0.43	−73
HF	37(12)	66(31)	0.58	78	29(31)	0.44	−22

Table 4
Same as Table 1, but for $PM_{2.5}$.

	OBS	MEIC			GE		
	Avg(σ)	Avg(σ)	R	MNB	Avg(σ)	R	MNB
NJ	100(59)	131 (87)	0.68	31	125(87)	0.67	25
LY	90(75)	80 (70)	0.84	−11	85(83)	0.84	−6
YZ	83(46)	116 (86)	0.80	40	110(86)	0.79	32
CZ	112(61)	148 (102)	0.77	32	142(99)	0.77	27
SH	82(63)	103 (86)	0.83	26	100(85)	0.81	22
HZ	90.6(50)	91.1 (58)	0.80	−0.6	85(59)	0.77	−6
NB	85(60)	69 (52)	0.84	−19	66(52)	0.84	−22
HF	104(55)	148 (79)	0.65	42	135(76)	0.68	30

inventory. Therefore, NO_x emissions from ocean surface near the coast are included in GlobEmission inventory. In addition, SO_2 emissions in GlobEmission are lower than MEIC over the entire YRD, but NO_x emissions in GlobEmission are lower than MEIC in some grids but higher in other grids. The differences range from −100% to 100% over YRD, with the mean value of −7%. The largest negative differences are found in Shanghai (45%), one of the first cities in China to implement strict regulations for vehicle emissions (Liu et al., 2016), followed by Hangzhou (16%) and Hefei (5%), while the lowest negative differences in Nanjing, only 4%.

3. Model description, observational data and model evaluation

3.1. Model description

The WRF-Chem model v3.6.1 (Grell, 2005) is used in this study to investigate the impact of two emission inventories on the simulated air pollutants over YRD. The simulation is performed on a domain in 27 km × 27 km horizontal resolution over eastern China and nested to a domain in 9 km × 9 km covering the YRD (Fig. 3), with 30 vertical levels. Gas-phase chemical mechanism CBMZ (Zaveri and Peters, 1999) and 4-bin sectional MOSAIC aerosol model with aqueous chemistry (Zaveri et al., 2008) are chosen. MOSAIC treats all the important aerosol species, including sulfate, nitrate, chloride, ammonium, sodium, BC, primary organic mass, liquid water, and other inorganic mass. Other parameterization schemes for physical processes include Morrison 2-moment (Morrison et al., 2008), RRTMG (Rapid Radiative Transfer Model for GCMs) short and long wave radiation (Iacono et al., 2008), Noah land surface model, and the Yonsei University planetary boundary layer parameterization (Hong et al., 2006). Initial meteorological conditions are obtained from the National Center for Environmental Prediction (NCEP) Final Analysis (FNL) dataset (http://rda.ucar.edu/datasets/ds083.2/) with a horizontal resolution of 1° × 1°. The chemical initial and boundary conditions are provided by the Model for Ozone and Related chemical Tracers, version 4 (MOZART-4) (Emmons et al., 2010). The emission data is interpolated into the model domain to generate hourly emission data, using the nearest neighbor interpolation method. As four haze episodes occurred and influenced multiple cities over YRD during January 2015, we selected this period for our study. The simulation started on 30 December 2014 and ended up on 31 January 2015, with the first 2 day as a spin-up.

3.2. Observational data

The meteorological conditions are key factors to control the

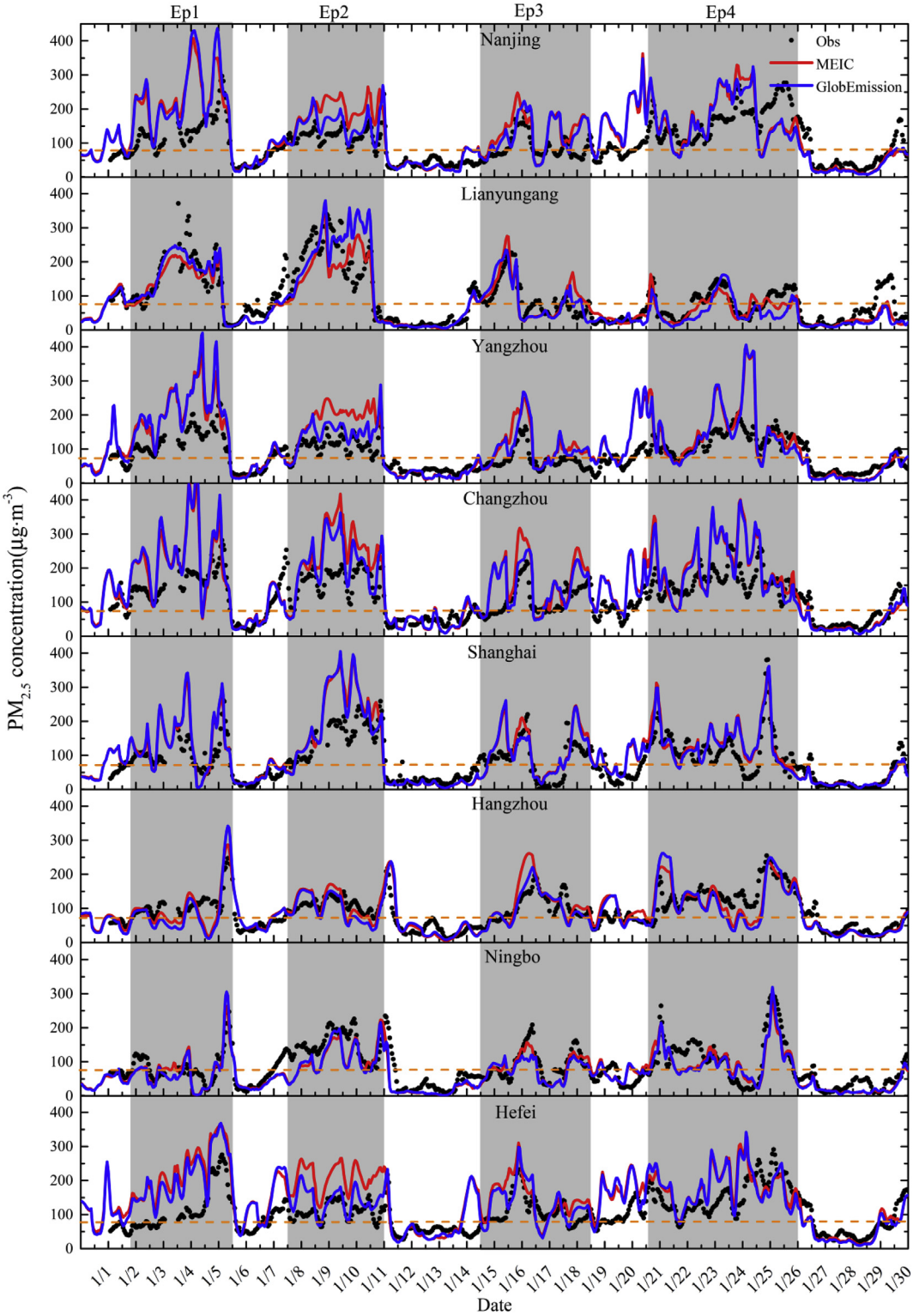

Fig. 8. Time series of observed (Obs) and simulated (using MEIC and GlobEmission inventories) hourly $PM_{2.5}$ in 8 cities of YRD. (The orange line in the graph represents the mass concentration of 75 μg m^{-3}). (For interpretation of the references to colour in this figure legend, the reader is referred to the Web version of this article.)

temporal and spatial distribution of the simulated air pollutants, it thus is essential to evaluate the modeled meteorological variables. The meteorological variables, such as 2 m temperature (T2), 2 m relative humidity (RH2), precipitation (PRE), 10 m wind speed (WS10) and wind direction (WD10), at 14, 13 and 16 meteorological stations in Shanghai, Nanjing and Hangzhou from Meteorological Information Comprehensive Analysis and Process System (MICAPS) (Gao et al., 2018), are used for evaluation in this study.

Starting from the year of 2013, the real-time hourly surface monitoring data on air quality, such as SO_2, NO_2, CO, O_3, $PM_{2.5}$, PM_{10} mass concentrations, are publicly released by the Ministry of Environmental Protection (MEP) in China (Zhang and Cao, 2015). We use the hourly

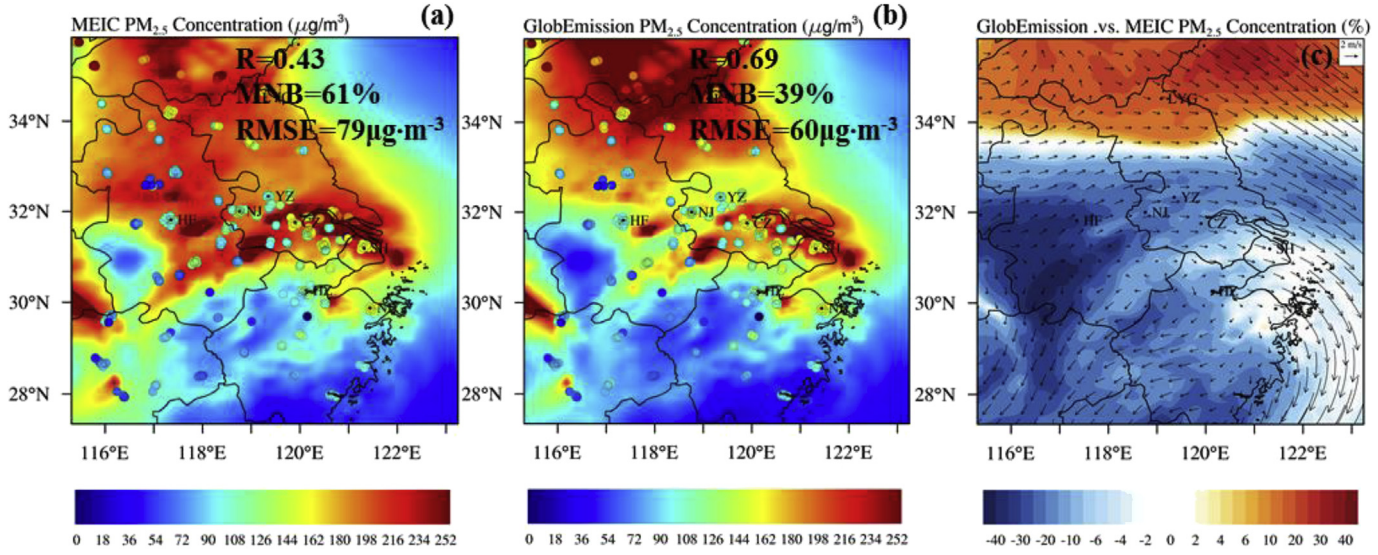

Fig. 9. Spatial distribution of simulated (using MEIC and GlobEmission inventories) and observed mean $PM_{2.5}$ (a, b) concentrations (unit: μg m^{-3}), and the relative differences of simulations (GlobEmission-MEIC)/MEIC × 100%) during haze event (Ep2: 8th to 11th January) over YRD (unit: %). The wind speed and wind direction are also plotted in Fig. (c). (The circles represent the observed air pollutants concentrations, and the black arrows indicate simulated surface wind fields.)

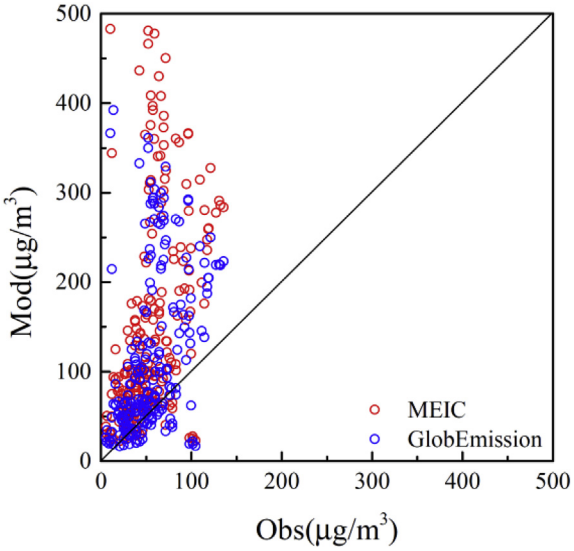

Fig. 10. Scatter plots of mean $PM_{2.5}$ concentrations between simulations and observations during haze event (Ep2: 8th to 11th January) over YRD (unit: μg m^{-3}). The black solid line in the graph is 1:1 line.

surface SO_2, NO_2, $PM_{2.5}$ concentrations from a total of 282 air quality monitoring sites of the MEP network over YRD (http://datacenter.mep.gov.cn), and the majority of these sites are located in the city center (MEP, 2013), which are required to be distributed in the developed area of the city and not too close to the stationary emission sources or roads (Liu et al., 2018). The location of sites is shown in Fig. 4. The model grid with one, two, three and four sites account for 60%, 26%, 12% and 2% to the total grids, respectively, so the mean values of observations from all sites in the same grid are compared with the results of model grids. In addition, hourly inorganic chemical components in $PM_{2.5}$ (sulfate, nitrate, ammonium) measured by the Monitor for AeRosols and GAses in ambient air (MARGA, Metrohm Applikon B.V., the Netherlands) (Brink et al., 2007) at Pudong site in Shanghai are also used (As the green solid circle shown in Fig. 4). Time periods of the observation data are all in January 2015.

3.3. Model evaluation

The statistical metrics, such as average and standard deviation, correlation coefficient (R), mean bias (MB), mean normalized bias (MNB) and root mean square error (RMSE), are used to evaluate the model performance. The definitions of these statistical quantities can be found in Morris et al. (2005) and Willmott and Matsuura (2005), the MNB and RMSE are calculated below:

$$\mathrm{MNB} = \frac{1}{n}\sum_{i=1}^{N}\left(\frac{sim_i - obs_i}{obs_i}\right) \quad (1)$$

$$\mathrm{RMSE} = \left[\frac{1}{n}\sum_{i=1}^{N}(sim_i - obs_i)^2\right]^{1/2} \quad (2)$$

in which *sim* and *obs* represent the simulated and observed values, and n is the number of samples.

As the differences in simulated meteorological fields based on two inventories are quite trivial (Fig. A1), only the simulations from MEIC are shown here. Fig. 5 compares the temporal variations of simulated and observed hourly temperature (ãc), relative humidity (d ~ f), precipitation (g ~ i), wind speed (j ~ l) and wind direction (m ~ o) at three cities (Shanghai, Nanjing, and Hangzhou) over YRD. Overall, the variations of surface temperature and relative humidity are captured quite well by the model, with correlation coefficients (R) in three cities of 0.88, 0.85, and 0.88 for surface temperature, and 0.72, 0.80, and 0.82 for relative humidity. As shown in Table 1, MB and RMSE of surface temperature vary from −0.8 °C to 1.0 °C and 2.18 °C–2.22 °C, respectively. The simulated relative humidity agrees well with observations, with MB and RMSE ranging from −11.0% to −0.7% and 13.3%–16.5%, respectively. Precipitation during this month is quite limited, and weak precipitation was found during January 13th to 14th in three cities, which the model can reproduce well. Wind speeds are overestimated throughout the entire period, especially in Shanghai, with positive MB and RMSE varying from 0.2 m s^{-1} to 2.5 m s^{-1} and 0.8 m s^{-1} to 2.8 m s^{-1}, respectively, which may cause some biases of the simulated air pollutants. The simulations of wind direction are basically consistent with measurements, with correlation coefficients (R) up to 0.63, 0.74, 0.56 at three cities, respectively.

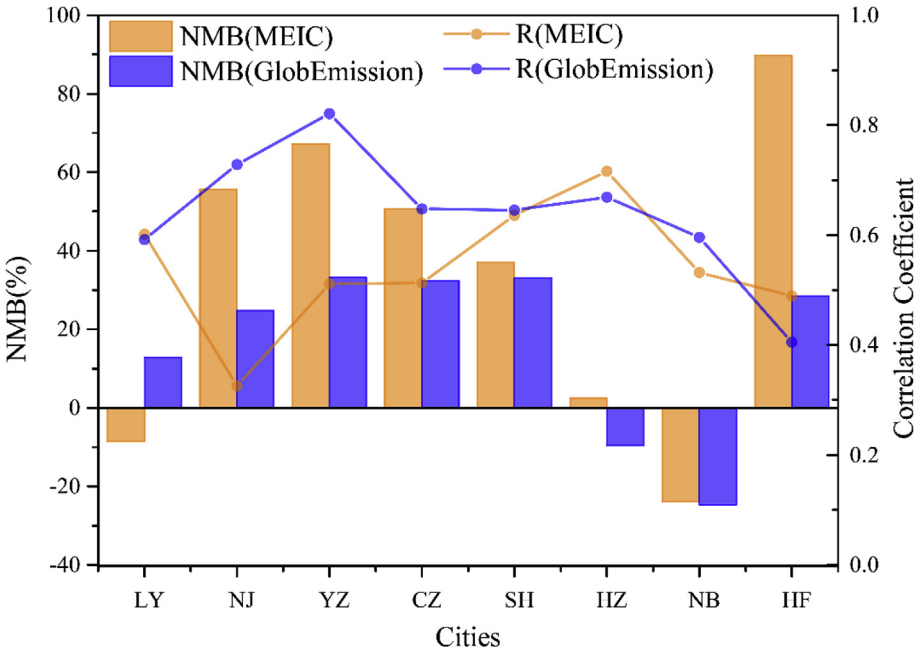

Fig. 11. Normalized mean bias (MNB) and correlation coefficients (R) of the simulated $PM_{2.5}$ concentrations using MEIC (orange) and GlobEmission inventory (blue) during haze event (Ep2: 8th to 11th January) in 8 cities of YRD. (For interpretation of the references to colour in this figure legend, the reader is referred to the Web version of this article.)

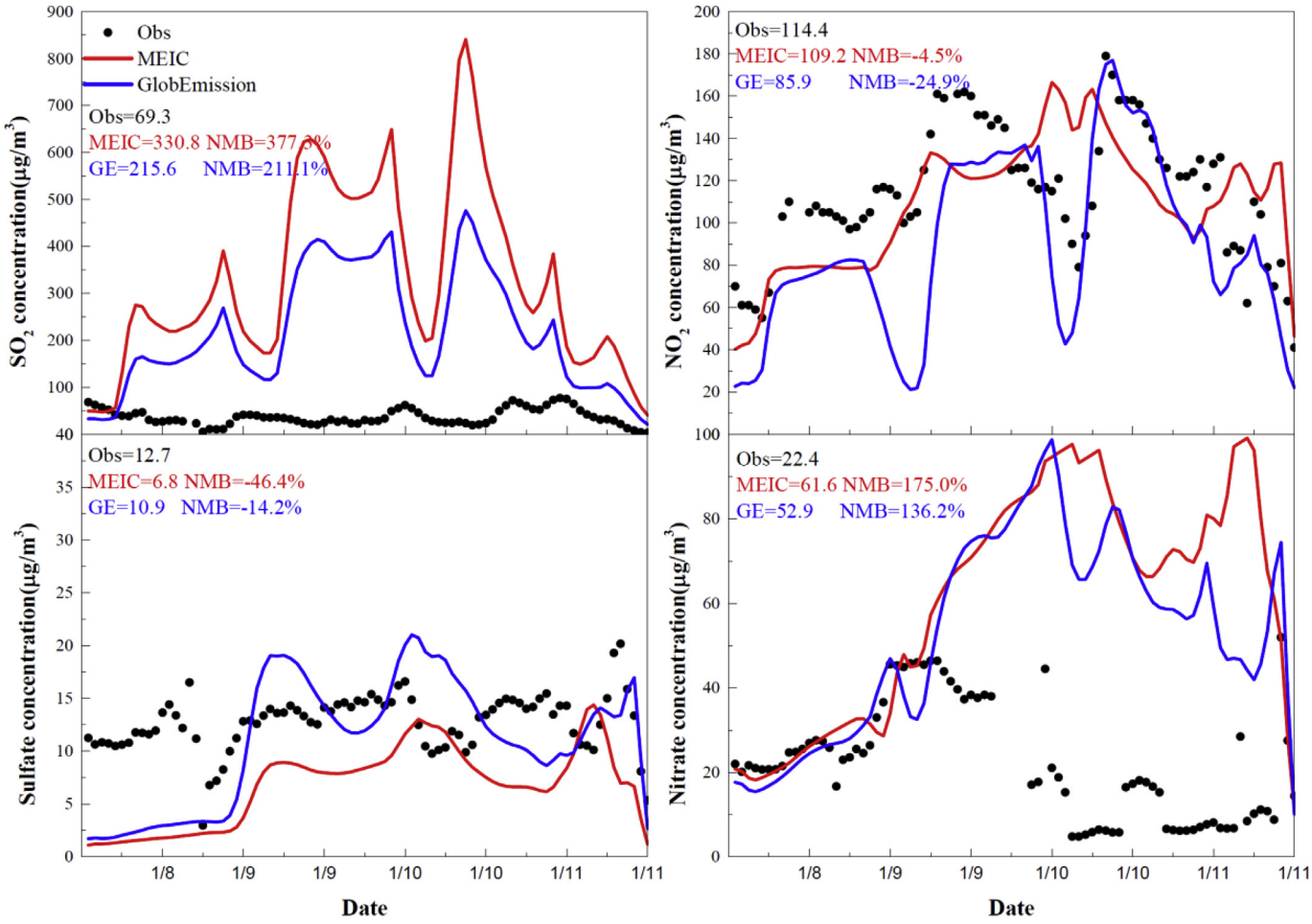

Fig. 12. Time series of observed (Obs) and simulated hourly SO_2, NO_2, sulfate, nitrate concentrations during haze event (Ep2: 8th to 11th January) at Pudong site in Shanghai.

4. Impacts of emission inventories on simulated air pollutants

4.1. Simulations based on two emission inventories

Fig. 6 shows that spatial distributions of monthly SO_2, NO_2, and $PM_{2.5}$ concentrations from the simulations using MEIC and GlobEmission, their relative differences (i.e. (GlobEmission-MEIC)/MEIC × 100%), as well as the observations. Overall, spatial distributions of the simulated air pollutants (SO_2, NO_2, and $PM_{2.5}$) are quite similar from two inventories, with high magnitudes in Southern Jiangsu and Northern Zhejiang province. For SO_2, spatial correlation coefficients between simulations and observations are only 0.27 (MEIC) and 0.30 (GlobEmission), respectively. Both MNB and RMSE are reduced by 86% and 30 $\mu g\,m^{-3}$ in the simulations with GlobEmission, possibly because SO_2 emissions in MEIC inventory have decreased by at least 30% during this period (2010–2015) (Chen et al., 2016; Krotkov et al., 2016). The simulations using GlobEmission and MEIC have larger difference (up to 117 $\mu g\,m^{-3}$) when SO_2 concentrations are higher than 20 $\mu g\,m^{-3}$, indicating that SO_2 emissions in polluted areas have been substantially reduced in recent years (Fig. 7a). The simulated SO_2 from both inventories are higher than the in-situ observations, especially in the polluted area including the city cluster of Nanjing-Shanghai. For instance, the simulations are nearly three (MEIC) and two times (GlobEmission) higher than observations in Nanjing (Table 2). The largest biases in comparisons to observations, either using MEIC or GlobEmission, are found in the city cluster of Nanjing-Shanghai, possibly indicating that SO_2 emissions are overestimated in both inventories. In addition, other physical and/or chemical processes may contribute to this discrepancy, such as underestimation dry and wet deposition of SO_2 and gas phase oxidation, the uncertainties of aqueous-phase chemistry, as well as missing heterogeneous sulfate formation in current model version. The biases between the simulations and in-situ observations in Zhejiang and Anhui province are relatively lower, with MNB of 104%, 168% (MEIC) and 46%, 89% (GlobEmission), respectively. It is shown that the standard deviation of SO_2 in 8 cities over YRD range from 11 to 26 $\mu g\,m^{-3}$ from the observed, while the standard deviations of simulations with two inventories are higher than that of observations (Table 2), indicating large variation SO_2 in the simulations.

On the contrary, the spatial correlation coefficient of the simulated NO_2 slightly increases from 0.43 to 0.49, and RMSE slightly reduces from 23 $\mu g\,m^{-3}$ to 21 $\mu g\,m^{-3}$ with MEIC than GlobEmission. The scatter plot (Fig. 7b) indicates that the simulations with MEIC overestimate while the simulations with GlobEmission underestimate the monthly mean NO_2 concentrations over YRD. Relative to observations, the biases of simulations using MEIC are less than 12% in most areas (Table 3). However, the simulations using GlobEmission are 22% lower than in-situ observations, with quite large negative biases found in Zhejiang province (over 70%). A few reasons possibly contribute to underestimations of NO_2. Firstly, the retrievals of NO_2 columns from OMI based on DOMINO v2 might have some disadvantages, such as biases in the calculation of air mass factor for retrievals at large solar zenith angles by the radiance transfer model and possibly biases in the estimated stratospheric background (Ding et al., 2017b; Liu et al., 2018; Lorente et al., 2017). Secondly, since aerosols have radiative impacts on tropospheric actinic flux, photolysis rates, and thus photochemical reactions rates associated with NO_x concentration (Mailler et al., 2017), an underestimation of $PM_{2.5}$ concentrations in the model might lead to strong actinic flux and reaction of NO_2 with OH, and thus weak NO_2 concentrations. Also, according to previous studies, NO_2 are measured using commercial chemiluminescence analyzers which are catalytically transformed into NO by a molybdenum converter and subsequently measured with chemiluminescence, and other reactive oxidized nitrogen compounds, such as alkyl nitrate (AN), peroxyacetyl nitrate (PAN) and HNO_3, are also partly converted to NO, resulting in an overestimation of measured NO_2, particularly at relatively clean regions and low latitudes (Steinbacher et al., 2007; Zhang and Cao, 2015; Liu et al., 2018). Therefore, the observed higher NO_2 may also cause large differences compared with the simulations.

The simulated monthly mean $PM_{2.5}$ concentrations using GlobEmission and MEIC show overall small differences, although large differences are found in simulated NO_2 (Fig. 7c). Overall, the simulated $PM_{2.5}$ using both inventories are both 20% higher than the observations in most areas, MNB and RMSE are reduced slightly (8% and 6 $\mu g\,m^{-3}$) over the whole YRD, and the spatial correlation coefficient is increased to 0.55 from 0.43, from the simulations with GlobEmission relative to MEIC. The standard deviations of simulations, as well as temporal correlation coefficients of observations and simulations using two inventories, are quite similar in 8 cities of YRD (Table 4). Earlier studies (Wang et al., 2014b; Chen et al., 2016; Gao et al., 2016a, b) indicated that missing heterogeneous sulfate formation in the current model might cause low gas-to-particle conversion and thus overestimation of SO_2 and underestimation of sulfate. Since SO_2 and NO_x compete for NH_3 in the atmosphere to convert to sulfate and nitrate, so lower conversion rate of SO_2 results in a large amount of free NH_3, which react with NO_x to produce nitrate. In addition, the simulated nitrate is much higher than the observations due to lower temperature in winter and relatively stable chemical properties of nitrate. As GlobEmission may underestimate the NO_x emissions in this area, the biases of simulated nitrate can be reduced to a certain extent, which leads to the biases of simulated $PM_{2.5}$ using GlobEmission are lower than when using MEIC.

4.2. Case studies of a haze event

The impact of emission inventories on the simulated air pollutants during winter over YRD have been studied in section 4.1. However, the monthly mean results possibly deviate the actual differences induced by two inventories to some extent due to the impact of long distance pollution transport. In this section, we focus on haze event in winter, which is mainly caused by local pollution, to further investigate the importance of inventories on the predicted haze status. According to the National Ambient Air Quality Standard (NAAQS) Grade II implemented in 2016 (GB3095-2012), a haze event is defined when daily average $PM_{2.5}$ mass concentration has reached or exceeded 75 $\mu g\,m^{-3}$ (Wang et al., 2014a). Four haze episodes were therefore determined during January 2015, including the episodes from 2nd to 6th (Ep1), 8th to 11th (Ep2), 16th to 18th (Ep3), and 21st to 26th (Ep4) (see Fig. 8), in which Ep1 and Ep3 were slight haze episodes, while Ep2 and Ep4 were moderate or heavy haze episodes. We choose Ep2 for a case study because it is more severe than Ep1 and Ep3, and time series of $PM_{2.5}$ and wind fields (see Fig. A2) indicate that Ep2 is mainly caused by local pollution, with relatively lower wind speeds (1.2 $m\,s^{-1}$) and shorter trajectories of air parcels, while Ep4 is mainly caused by long distance transportation of air pollutants, with relatively higher wind speeds (2.2 $m\,s^{-1}$) and much longer trajectories of air parcels (see Fig. A3 and Fig. A4).

Spatial distributions of $PM_{2.5}$ concentrations during Ep2 from observations and simulations, and the relative differences of the simulations from two inventories, i.e. (GlobEmission-MEIC)/MEIC × 100%), are shown in Fig. 9. As expected, the mean $PM_{2.5}$ concentrations during haze event are 51% higher than the monthly mean (Table 4 and A1), due to much lower wind speed (1.2 $m\,s^{-1}$) which facilitates the rapid accumulation and increase for air pollutants. The simulations with both GlobEmission and MEIC overestimate observed $PM_{2.5}$ concentrations over YRD (Figs. 9 and 10). The MNB and RMSE of are 61% and 79 $\mu g\,m^{-3}$ in the simulation using MEIC, and 39% and 60 $\mu g\,m^{-3}$ in the simulation using GlobEmission. Additionally, spatial correlation coefficient in the simulation using GlobEmission increase to 0.69.

As shown in Fig. 11, the NMBs of the simulated PM2.5 are overall lower in the simulations using GlobEmission than MEIC for most cities of YRD. For example, the city cluster of Nanjing-Shanghai, where the

biases are reduced to 25%–33% from 37% to 67% and temporal correlation coefficients are increased to 0.7 from 0.5, in the simulations using GlobEmission, compared with the simulations using MEIC.

Fig. 12 shows the temporal variations of two major gas precursors (SO_2, NO_2) and inorganic components in $PM_{2.5}$ (sulfate, nitrate) at Pudong site in Shanghai. It is seen that the simulated SO_2 from MEIC (GlobEmission) is nearly four (two) times as large as observations, and the biases of simulated sulfate is 32% lower in the simulation with GlobEmission than with MEIC. The simulated NO_2 using MEIC and GlobEmission is 4.5% and 24.9% lower than observations, respectively. The simulated nitrates from both emission inventories are all higher than observations, but the bias with GlobEmission is reduced by 39%. The overestimation of SO_2 and underestimation of sulfate in the simulations imply that the parameterizations of sulfate formation might be problematic in current model version.

5. Summary and conclusions

To understand the impact of different emission inventories on the simulated air pollutants, two inventories, MEIC and GlobEmission, representing the emission inventories based on quite different ways, are involved in this study. MEIC is based on typical bottom-up approach while GlobEmission is representative of top-down inventory, in which the emissions are estimated from satellite retrievals. We first compared the monthly emissions of SO_2 and NO_x in two inventories over YRD, and found that the differences of emissions between two inventories are quite large. The differences of SO_2 in two inventories are dependent on regional division, i.e. the emission from GlobEmission is 47%, 29%, and 16% lower than MEIC in Shanghai, Anhui province, and Zhejiang province, respectively. The differences of NO_x emissions in two inventories vary in each grid cell due to totally different approaches used for estimations of emission. The largest NO_x difference is found in Shanghai (45%), followed by Hangzhou (16%) and the lowest in Nanjing (4%).

A quantitative model evaluation of meteorological fields in three cities (Shanghai, Nanjing, and Hangzhou) over YRD shows that the model can capture the temporal variations of surface temperature, relative humidity, precipitation, wind speed and wind direction quite well. The biases of simulations are overall small, except for wind speeds, which are overestimated throughout the entire period and may possibly cause some biases of the simulated air pollutants.

The WRF-Chem model is used to study the impact of discrepancies in different inventories on simulated air pollutants (SO_2, NO_2, $PM_{2.5}$) during January 2015, and a selected heavy haze event over YRD. Overall, the simulations of two inventories can both capture the temporal and spatial variation of major air pollutants. Although the simulations of SO_2 using GlobEmission reduce MNB and RMSE by more than 80% and 30 $\mu g\,m^{-3}$, respectively, the largest deviations between simulations and observations exist in the city cluster of Nanjing-Shanghai, where the simulations are nearly four (MEIC) and three times (GlobEmission) as large as observations, possibly indicating an overestimation of SO_2 emissions in both inventories, and a difference existing between the baseline year of inventories and the simulations. Another possible explanation is that the current model version does not include heterogeneous sulfate formation, which may underestimate the conversion rate from SO_2 to sulfate. On the contrary, compared with the simulations by using GlobEmission, the NO_2 simulations using MEIC slightly increase spatial correlation coefficient from 0.43 to 0.49, and reduce RMSE from 23 $\mu g\,m^{-3}$ to 21 $\mu g\,m^{-3}$. The mean biases using MEIC are less than 12% in most regions, while the simulations of GlobEmission are 22% lower than in-situ observations, especially in Zhejiang province, where the negative biases of simulation are more than 70%, possibly indicating that GlobEmission underestimates NO_x emissions in this area. The simulated monthly mean $PM_{2.5}$ are 38% (MEIC) and 30% (GlobEmission) higher than in-situ observations over YRD.

A case study during a heavy haze event (8th to 11th in January) shows that the differences in simulated mean $PM_{2.5}$ between using two inventories are 22% (MNB) and 19 $\mu g\,m^{-3}$ (RMSE) over YRD, which are larger than the monthly mean results (8% for MNB and 6 $\mu g\,m^{-3}$ for RMSE), indicating importance of choosing emission inventories in simulations of haze pollution. Compared to the simulations with MEIC inventory, the spatial correlation coefficient between observations and simulations increase 0.43 to 0.69 over YRD, and temporal correlation coefficients increase from 0.5 to 0.7 in the city cluster of Nanjing-Shanghai, by using GlobEmission inventory.

Declaration of interest statement

We declare that we do not have any commercial or associative interest that represents a conflict of interest in connection with the manuscript submitted.

Acknowledgments

This study is supported by the National Natural Science Foundation of China grants (41675004) and the National Key R&D Program of China grants (2016YFA0600404).

References

Boersma, K.F., Eskes, H.J., Dirksen, R.J., van der A, R.J., Veefkind, J.P., Stammes, P., Huijnen, V., Kleipool, Q.L., Sneep, M., Claas, J., Leitão, J., Richter, A., Zhou, Y., Brunner, D., 2011. An improved tropospheric NO_2 column retrieval algorithm for the Ozone Monitoring Instrument. Atmospheric Measurement Techniques 4, 1905–1928.

Brink, H.T., Otjes, R., Jongejan, P., Slanina, S., 2007. An instrument for semi-continuous monitoring of the size-distribution of nitrate, ammonium, sulphate and chloride in aerosol. Atmos. Environ. 41 (13), 2768–2779.

Chang, L.Y., Xu, J.M., Zhou, G.Q., Wu, J.B., Xie, Y., Yu, Z.Q., Yang, C., 2016. A numerical study of typical heavy air pollution episode of $PM_{2.5}$ in Shanghai. Environ. Sci. 37 (3), 825–833 (in Chinese).

Chen, D., Liu, Z.Q., Fast, J., Ban, J., 2016. Simulations of sulfate–nitrate–ammonium (SNA) aerosols during the extreme haze events over northern China in October 2014. Atmos. Chem. Phys. 16, 10707–10724.

Cheng, Y.F., Zheng, G.J., Wei, C., Mu, Q., Zheng, B., Wang, Z.B., Gao, M., Zhang, Q., He, K.B., Carmichael, G., Pöschl, U., Su, H., 2016. Reactive nitrogen chemistry in aerosol water as a source of sulfate during haze events in China. Science Advances 2 (12).

Chimot, J., Vlemmix, T., Veefkind, J.P., de Haan, J.F., Levelt, P.F., 2016. Impact of aerosols on the OMI tropospheric, NO_2 retrievals over industrialized regions: how accurate is the aerosol correction of cloud-free scenes via a simple cloud model? Atmospheric Measurement Techniques 9, 359–382.

Ding, J.Y., Miyazaki, K., van der A, R.J., Mijling, B., Kurokawa, J.I., Cho, S.Y., Janssens-Maenhout, G., Zhang, Q., Liu, F., Levelt, P.F., 2017a. Intercomparison of NO_x emission inventories over east Asia. Atmos. Chem. Phys. 17, 10125–10141.

Ding, J.Y., van der A, R.J., Mijling, B., Levelt, P.F., 2017b. Space-based NO_x emission estimates over remote regions improved in DECSO. Atmospheric Measurement Techniques 10, 925–938.

Ding, J.Y., van der A, R.J., Mijling, B., Levelt, P.F., Hao, N., 2015. NO_x emission estimates during the 2014 youth olympic games in Nanjing. Atmos. Chem. Phys. 15, 9399–9412.

Emmons, L.K., Walters, S., Hess, P.G., Lamarque, J.F., Pfister, G.G., Fillmore, D., Granier, C., Guenther, A., Kinnison, D., Laepple, T., Orlando, J., Tie, X., Tyndall, G., Wiedinmyer, C., Baughcum, S.L., Kloster, S., 2010. Description and evaluation of the model for ozone and related chemical Tracers, version 4 (MOZART-4). Geosci. Model Dev. (GMD) 3, 43–67.

Fu, X., Cheng, Z., Wang, S.X., Hua, Y., Xing, J., Hao, J.M., 2016a. Local and regional contributions to fine particle pollution in winter of the Yangtze River Delta, China. Aerosol and Air Quality Research 16 (4), 1067–1080.

Fu, X., Wang, S.X., Chang, X., Cai, S.Y., Xing, J., Hao, J.M., 2016b. Modeling analysis of secondary inorganic aerosols over China: pollution characteristics, and meteorological and dust impacts. Sci. Rep. 6 (1), 35992.

Gao, J.H., Zhu, B., Xiao, H., Kang, H.Q., Pan, C., Wang, D.D., Wang, H.L., 2018. Effects of black carbon and boundary layer interaction on surface ozone in Nanjing, China. Atmos. Chem. Phys. 18 (10), 7081–7094.

Gao, M., Carmichael, G.R., Wang, Y.S., Ji, D.S., Liu, Z.R., Wang, Z.F., 2016a. Improving simulations of sulfate aerosols during winter haze over Northern China: the impacts of heterogeneous oxidation by NO_2. Front. Environ. Sci. Eng. 10 (5), 165–175.

Gao, M., Carmichael, G.R., Wang, Y.S., Saide, P.E., Yu, M., Xin, J., Liu, Z.R., Wang, Z.F., 2016b. Modeling study of the 2010 regional haze event in the North China Plain. Atmos. Chem. Phys. 16, 1673–1691.

Grell, G.A., Peckham, S.E., Schmitz, R., Mckeen, S.A., Frost, G., Skamarock, W.C., Eder, B., 2005. Fully coupled "online" chemistry within the WRF model. Atmos. Environ. 39 (37), 6957–6975.

Guo, H., Weber, R.J., Nenes, A., 2017. High levels of ammonia do not raise fine particle

pH sufficiently to yield nitrogen oxide-dominated sulfate production. Sci. Rep. 7, 12109.
Hong, S.Y., Noh, Y., Dudhia, J., 2006. A new vertical diffusion package with an explicit treatment of entrainment processes. Mon. Weather Rev. 134 (9), 2318.
Iacono, M.J., Delamere, J.S., Mlawer, E.J., Shephard, M.W., Clough, S.A., Collins, W.D., 2008. Radiative forcing by long-lived greenhouse gases: calculations with the AER radiative transfer models. J. Geophys. Res.: Atmosphere 113 (D13).
Koukouli, M.E., Theys, N., Ding, J.Y., Zyrichidou, I., Balis, D., van der A, R.J., 2017. Top-Down SO2 Emissions over China; A Satellite Approach. Comecap2016 Conference, September 2016. T. Karacostas Et Al.
Krotkov, N.A., McLinden, C.A., Li, C., Lamsal, L.N., Celarier, E.A., Marchenko, S.V., Swartz, W.H., Bucsela, E.J., Joiner, J., Duncan, B.N., Boersma, K.F., Veefkind, J.P., Levelt, P.F., Fioletov, V.E., Dickerson, R.R., He, H., Lu, Z., Streets, D.G., 2016. Aura OMI observations of regional SO_2 and NO_2 pollution changes from 2005 to 2015. Atmos. Chem. Phys. 16, 4605–4629.
Li, G.H., Bei, N.F., Cao, J.J., Huang, R.J., Wu, J.R., Feng, T., Wang, Y.C., Liu, S.X., Zhang, Q., Tie, X.X., Molina, L.T., 2017a. A possible pathway for rapid growth of sulfate during haze days in China. Atmos. Chem. Phys. 17, 3301–3316.
Li, M., Klimont, Z., Zhang, Q., Martin, R.V., Zheng, B., Heyes, C., Cofala, J., Zhang, Y.X., He, K.B., 2018. Comparison and evaluation of anthropogenic emissions of SO_2 and NO_x over China. Atmos. Chem. Phys. 18 (5), 3433–3456.
Li, M., Zhang, Q., Kurokawa, J., Woo, J.H., He, K.B., Lu, Z.F., Ohara, T., Song, Y., Streets, D.G., Carmichael, G.R., Cheng, Y.F., Hong, C.P., Huo, H., Jiang, X.J., Kang, S., Liu, F., Su, H., Zheng, B., 2017b. MIX: a mosaic Asian anthropogenic emission inventory under the international collaboration framework of the MICS-Asia and HTAP. Atmos. Chem. Phys. 17, 935–963.
Liu, F., van der A, R.J., Eskes, H., Ding, J.Y., Mijling, B., 2018. Evaluation of modeling NO_2 concentrations driven by satellite-derived and bottom-up emission inventories using in-situ measurements over China. Atmospheric Chemistry and Physics. 2017 1–25.
Liu, F., Zhang, Q., Tong, D., Zheng, B., Li, M., Huo, H., He, K.B., 2015. High-resolution inventory of technologies, activities, and emissions of coal-fired power plants in China from 1990 to 2010. Atmos. Chem. Phys. 15 (23), 13299–13317.
Liu, F., Zhang, Q., van, d. A.R.J., Zheng, B., Tong, D., Yan, L., Zheng, Y.X., He, K.B., 2016. Recent reduction in NO_x emissions over China: synthesis of satellite observations and emission inventories. Environ. Res. Lett. 11 (14), 3945–3950.
Lorente, A., Folkert Boersma, K., Yu, H., Dörner, S., Hilboll, A., Richter, A., Liu, M., Lamsal, L.N., Barkley, M., De Smedt, I., Van Roozendael, M., Wang, Y., Wagner, T., Beirle, S., Lin, J.-T., Krotkov, N., Stammes, P., Wang, P., Eskes, H.J., Krol, M., 2017. Structural uncertainty in air mass factor calculation for NO_2 and HCHO satellite retrievals. Atmospheric Measurement Techniques 10 (3), 1–35.
Lu, Z.Y., Zhang, Q., Streets, D.G., 2011. Sulfur dioxide and primary carbonaceous aerosol emissions in China and India, 1996–2010. Atmos. Chem. Phys. 11, 9839–9864.
Mailler, S., Menut, L., Khvorostyanov, D., Valari, M., Couvidat, F., Siour, G., Turquety, S., Briant, R., Tuccella, P., Bessagnet, B., Colette, A., Létinois, L., Markakis, K., Meleux, F., 2017. CHIMERE-2017: from urban to hemispheric chemistry-transport modeling. Geosci. Model Dev. (GMD) 10 (6), 2397–2423.
Mijling, B., van der A, R.J., 2012. Using daily satellite observations to estimate emissions of short-lived air pollutants on a mesoscopic scale. J. Geophys. Res.: Atmosphere 117 (D17).
Mijling, B., van der A, R.J., Zhang, Q., 2013. Regional nitrogen oxides emission trends in East Asia observed from space. Atmos. Chem. Phys. 13, 12003–12012.
Ministry of Environmental Protection of the People's Republic of China (MEP), 2013. Technical regulation for selection of ambient air quality monitoring stations (on trial). available at: http://kjs.mep.gov.cn/hjbhbz/bzwb/jcffbz/201309/t20130925_260810.shtml (last access: 1 May 2017) (in Chinese).
Morris, R.E., McNally, D.E., Tesche, T.W., Tonnesen, G., Boylan, J.W., Brewer, P., 2005. Preliminary evaluation of the community multiscale air quality model for 2002 over the southeastern United States. Air Waste Manage 55, 1694–1708. https://doi.org/10.1080/10473289.2005.10464765.
Morrison, H., Pinto, J.O., Curry, J.A., McFarquhar, G.M., 2008. Sensitivity of modeled arctic mixed-phase stratocumulus to cloud condensation and ice nuclei over regionally varying surface conditions. J. Geophys. Res.: Atmosphere 113 (D5).
Saikawa, E., Kim, H., Zhong, M., Avramov, A., Zhao, Y., Janssens-Maenhout, G., Kurokawa, J., Klimont, Z., Wagner, F., Naik, V., Horowitz, L.W., Zhang, Q., 2017. Comparison of emissions inventories of anthropogenic air pollutants and greenhouse gases in China. Atmos. Chem. Phys. 17 (10), 6393–6421.
Shaiganfar, R., Beirle, S., Sharma, M., Chauhan, A., Singh, R.P., Wagner, T., 2011. Estimation of NO_x emissions from Delhi using Car MAX-DOAS observations and comparison with OMI satellite data. Atmos. Chem. Phys. 11 (7), 10871–10887.
Steinbacher, M., Zellweger, C., Schwarzenbach, B., Bugmann, S., Buchmann, B., Ordonez, C., Prevot, A.S.H., Hueglin, C., 2007. Nitrogen oxide measurements at rural sites in Switzerland: bias of conventional measurement techniques. J. Geophys. Res.: Atmosphere 112, D11307.
Sun, K., Liu, H.N., Ding, A.J., Wang, X.Y., 2016. WRF-chem simulation of a severe haze episode in the Yangtze River Delta, China. Aerosol and Air Quality Research 16 (5), 1268–1283.
Theys, N., De Smedt, I., Van Gent, J., Danckaert, T., Wang, T., Hendrick, F., Stavrakou, T., Bauduin, S., Clarisse, L., Li, C., Krotkov, N., Yu, H., Brenot, H., Van Roozendael, M., 2015. Sulfur dioxide vertical column DOAS retrievals from the Ozone Monitoring Instrument: global observations and comparison to ground-based and satellite data. J. Geophys. Res.: Atmosphere 120 (6), 2470–2491.
van, d.A.R.J., Mijling, B., Ding, J.Y., Elissavet Koukouli, M., Liu, F., Li, Q., Mao, H.Q., Theys, N., 2017. Cleaning up the air: effectiveness of air quality policy for SO2 and NOx emissions in China. Atmos. Chem. Phys. 17 (3), 1–18. https://doi.org/10.5194/acp-17-1775-2017.
Wang, G.H., Zhang, R.Y., Gomez, M.E., Yang, L.X., Zamora, M.L., Hu, M., Lin, Y., Peng, J.F., Guo, S., Meng, J.J., Li, J.J., Cheng, C.L., Hu, T.F., Ren, Y.Q., Wang, X.S., Gao, J., An, Z.S., Zhou, W.J., Li, G.H., Wang, J.Y., Tian, Y.Q., Marrero-Ortiz, W., Secrest, J., Du, Z.F., Zheng, J., Dongjie, S., Zeng, L., Shao, M., Wang, W.G., Huang, Y., Wang, Y., Zhu, Y.J., Li, Y.X., Hu, J.X., Pan, B., Cai, L., Cheng, Y.T., Ji, Y.M., Zhang, F., Rosenfeld, D., Liss, P.S., Duce, R.A., Kolb, C.E., Molina, M.J., 2016. Persistent sulfate formation from London Fog to Chinese haze. Proc. Natl. Acad. Sci. U.S.A. 48 (113), 13630–13635.
Wang, J., Shi, R.H., Li, L., Zhang, L., 2015a. Characteristics and formation mechanism of a heavy air pollution episode in Shanghai. Acta Sci. Circumstantiae 35 (5), 1537–1546 (in Chinese).
Wang, S.W., Zhang, Q., Martin, R.V., Philip, S., Liu, F., Li, M., Jiang, X.J., He, K.B., 2015b. Satellite measurements over-see China's sulfur dioxide emission reductions from coal-fired power plants. Environ. Res. Lett. 10, 114015.
Wang, Y.S., Yao, L., Wang, L.L., Liu, Z.R., Ji, D.S., Tang, G.Q., Zhang, J.K., Sun, Y., Hu, B., Xin, J.Y., 2014a. Mechanism for the formation of the January 2013 heavy haze pollution episode over central and eastern China. Sci. China Earth Sci. 57 (1), 14–25.
Wang, Y.X., Zhang, Q.Q., Jiang, J.K., Zhou, W., Wang, B.Y., He, K.B., Duan, F.K., Zhang, Q., Philip, S., Xie, Y.Y., 2014b. Enhanced sulfate formation during China's severe winter haze episode in January 2013 missing from current models. J. Geophys. Res.: Atmosphere 119 (17), 10425–10440.
Willmott, C.J., Matsuura, K., 2005. Advantages of the mean absolute error (MAE) over the root mean square error (RMSE) in assessing average model performance. Clim. Res. 30, 79–82.
Xia, Y., Zhao, Y., Nielsen, C.P., 2016. Benefits of China's efforts in gaseous pollutant control indicated by the bottom-up emissions and satellite observations 2000-2014. Atmos. Environ. 136, 43–53.
Zaveri, R.A., Easter, R.C., Fast, J.D., Peters, L.K., 2008. Model for simulating aerosol interactions and chemistry (MOSAIC). J. Geophys. Res.: Atmosphere 113.
Zaveri, R.A., Peters, L.K., 1999. A new lumped structure photochemical mechanism for large-scale applications. J. Geophys. Res.: Atmosphere 104, 30387–30415.
Zhang, Q., Geng, G.N., Wang, S.W., Richter, A., He, K.B., 2012. Satellite remote sensing of changes in NO_x emissions over China during 1996–2010. Chin. Sci. Bull. 57, 2857–2864.
Zhang, X., Xu, J.M., Wang, T.J., Zhu, J.L., 2015. Characteristics and formation mechanism of a serious haze episode in December 2013 in Shanghai. Journal of Nanjing University (Natural Sciences) 51 (3), 463–472 (in Chinese).
Zhang, X., Zhang, W., Lu, X., Liu, X., Chen, D., Liu, L., Huang, X., 2018. Long-term trends in NO_2 columns related to economic developments and air quality policies from 1997 to 2016 in China. Sci. Total Environ. 639, 146–155.
Zhang, Y.L., Cao, F., 2015. Fine particulate matter ($PM_{2.5}$) in China at a city level. Sci. Rep. 5, 14884. https://doi.org/10.1038/srep14884.
Zhao, Y., Zhang, J., Nielsen, C.P., 2014. The effects of energy paths and emission controls and standards on future trends in China's emissions of primary air pollutants. Atmos. Chem. Phys. 14, 8849–8868. https://doi.org/10.5194/acp-14-8849-2014.
Zheng, B., Huo, H., Zhang, Q., Yao, Z.L., Wang, X.T., Yang, X.F., Liu, H., He, K.B., 2014. High-resolution mapping of vehicle emissions in China in 2008. Atmos. Chem. Phys. 14, 9787–9805. https://doi.org/10.5194/acp-14-9787-2014.
Zheng, L.F., Xie, Y.N., Liu, Q., Huang, X., Nie, W., Ding, A.J., 2016. Heavy haze events during december 2013 in Nanjing. Transactions of Atmospheric Sciences 39 (4), 546–553 (in Chinese).
Zhou, G.Q., Xu, J.M., Xie, Y., Chang, L.Y., Gao, W., Gu, Y.X., Zhou, J., 2017. Numerical air quality forecasting over eastern China: an operational application of WRF-Chem. Atmos. Environ. 153, 94–108.